J Mater Sci (2008) 43:4938–4944
DOI 10.1007/s10853-008-2720-0

Transient liquid phase bonding of steel using an Fe–B interlayer: microstructural analysis

N. Di Luozzo · M. Fontana · B. Arcondo

Received: 7 December 2007 / Accepted: 12 May 2008 / Published online: 30 May 2008

Abstract Transient liquid phase bonding processes have been performed to join two carbon steel tubes using $Fe_{96.2}B_{3.8}$ wt% amorphous ribbons as interlayer. Welding experiments were performed at the temperature $T \approx$ 1,250 °C for different durations and under pressures of 0.8, 2, 3, and 4 MPa. From metallographic inspection, it is concluded that the bonding process ends in 7.0 min if a pressure of 4 MPa is applied, whereas the process results incomplete if less pressure is applied. The metallurgical aspects of these joints are analyzed. Plastic deformation at the joint is observed. Micrographs show that if pressure increases, the amount of pro-eutectoid ferrite decreases, therefore, an increase in the hardenability of the steel occurs. This fact could be due to the effect of the compression plastic deformation that prevails at the joint zone.

Introduction

In recent years, the transient liquid phase bonding (TLPB) process has been widely studied [1–4] in order to improve the characteristics of the joints by means of composition and microstructure homogenization along the joined pieces. TLPB is commonly used in the repair of aeroengine turbine blades and involves three main steps, namely, liquefaction of the filler material and base metal dissolution in the liquid gap, liquid phase isothermal solidification, and solute homogenization [5–7]. TLPB of Ni-based superalloys [6], steel [8–10] with different composition interlayers and under different conditions have been performed.

In a previous work [11], a numerical model was used to research TLPB of steel/iron–boron/steel under different pressures. We observed that the effect of pressure is to reduce the isothermal stage time. This fact is due to liquid ejection from the joining zone as well as to the softening of the roughness of the metal surfaces.

In this study, we continue analyzing the bonds using optical microscopy (OM), scanning electron microscopy (SEM), and energy dispersive X-ray analyses (EDX). The aim is to study the microstructure of the bonds, composition, and morphology of the joint and how the different parameters influence them.

A brief physical description of the TLPB process is explained in the following sections "Physical description," "Experimental procedure," "Experimental results," "Discussion," and "Conclusions."

Physical description

Let us assume that two tubes of a solid γ (with composition C_S) are aligned with their surfaces in contact with a thin amorphous layer of thickness a. The amorphous layer composition C_L is not far from a eutectic point (E) whose components are γ and β (Fig. 1). The melting temperature of the amorphous layer (T_L) is lower than the melting temperature of γ (T_S). If the temperature in the joining zone is raised to T_p at the highest possible rate, being $T_L < T_p < T_S$, a

N. Di Luozzo
Tenaris University Industrial School, Tenaris, Dr. Simini 250, Campana 2804, Argentina
e-mail: ndiluozzo@tenaris.com

M. Fontana · B. Arcondo (✉)
Laboratorio de Solidos Amorfos, Instituto de Tecnologias y Ciencias de la Ingenieria, Facultad de Ingenieria, Universidad de Buenos Aires-CONICET, Paseo Colon 850, Buenos Aires 1063, Argentina
e-mail: barcond@fi.uba.ar

M. Fontana
e-mail: mfontan@fi.uba.ar

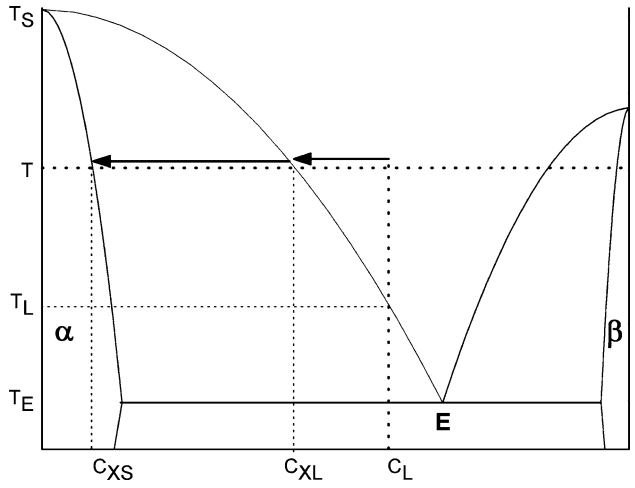

Fig. 1 Phase equilibrium diagram of the α–β system. T is the isothermal welding temperature, C_L the initial composition of the transient liquid gap, C_{XL} the composition of the liquid gap as a solid phase of composition C_{XS} precipitates

transient liquid phase forms. As the temperature T is held constant, the following process will take place:

- The dissolution of the base material into the liquid gap occurs, thus widening the gap.
- When the concentration in the liquid reaches C_{XL}, the solidification starts and the gap proceeds to close up to its total disappearance (the concentration of the solid in the interface is C_{XS}).
- The completion of the solid-state diffusion is performed [7, 12].

The amorphous nature of the layer is not a precondition for the TLPB process. However, amorphous layers present many advantages when compared to the corresponding crystalline materials. Metallic glasses have a very large ductility therefore, in the form of thin layers; amorphous metals are easier to handle than crystals. In addition, amorphous layers improve the contact with the tubes when pressure is applied, whereas crystalline layers break.

Experimental procedure

TLPB processes under Ar atmosphere have been performed to join two carbon steel tubes (see composition in Table 1) of 19 mm external diameter and 2.5 mm wall thickness. $Fe_{96.2}B_{3.8}$ wt.% amorphous ribbons of thickness $a = 20$ μm have been employed as interlayer. The tubes were aligned with the surfaces of both pieces in contact with the amorphous layer. The surfaces were prepared by turning and its average roughness is $R_a = 1.6$ μm on an evaluation length of 2.5 mm with a cut-off length of 2.5 mm. The arrangement was placed into the coil of an induction furnace under Ar atmosphere. The temperature was raised at the highest possible rate to T_p (with T_p about 1,250 °C) and then held constant for different times. The welding processes were performed under pressures P of 0.8, 2, 3, and 4 MPa. The duration of the welding processes was up to 17.0 min for $P = 0.8$ MPa and up to 7.0 min for higher pressures. Several samples were obtained for each set of parameters.

Table 1 Steel tubes composition (wt%)

C	Mn	Si	Ni	Cr	Mo	Cu	B
0.120	0.450	0.180	0.025	0.030	0.010	0.054	0.0001
Sn	V	Al	Nb	Ti	As	S	P
0.004	0.001	0.025	0.001	0.001	0.003	0.0019	0.011

The outer surface of the joined tubes was mechanically smoothed parallel to the axis of the tubes in order to prepare a 12 mm (width) 30 mm (length) plane surface where the microstructure of the joint region resulted exposed. The width of the plane surface displays the microstructure at different depths into the tube wall; the external borders correspond to the outer surface of the tubes, whereas the central line corresponds to the through-wall depths of the tube (~2.1 mm from the outer surface). The plane surface was polished with emery paper and micropolished with 0.05-μm gamma alumina. These surfaces were examined using OM, SEM, and EDX (Philips XL 30CP).

Experimental results

Micrographs of the tubes of as received condition (before the bonding process) obtained using SEM are shown in Fig. 2. The structure observed employing secondary electrons consists of spheroidal cementite particles (white) in a matrix of ferrite (dark). Micrographs obtained with backscattered electrons show a random distribution of spheroidal particles, each about 6 μm or less (the presence of Fe, Al, O, Si, S, Ca, Mn, and Mg is detected using EDX).

The SEM micrographs of the tubes after the bonding process performed with $P = 0.8$ MPa and a holding time of 3 min at T_P are shown in Fig. 3. This figure shows a non-isothermally solidified liquid (NSL) at the joint line. This phase is due to the incomplete solidification of the gap in the holding time. The composition analyses of NSL using EDX show only Fe (B cannot be detected by this technique). At the through-wall depths of the tube, micrographs show a distribution of particles, each about 1–5 μm in diameter, laying mainly at prior austenite grain boundaries (the presence of Fe, Al, O, S, Ca, Mn, and Mg is detected using EDX). A random distribution of spheroidal particles, each about 5 μm or less (the presence of Fe, Al, O, Si, S, Ca, and Mg is confirmed using EDX), is observed at 10 mm from the joint, at the through-wall depths of the tube.

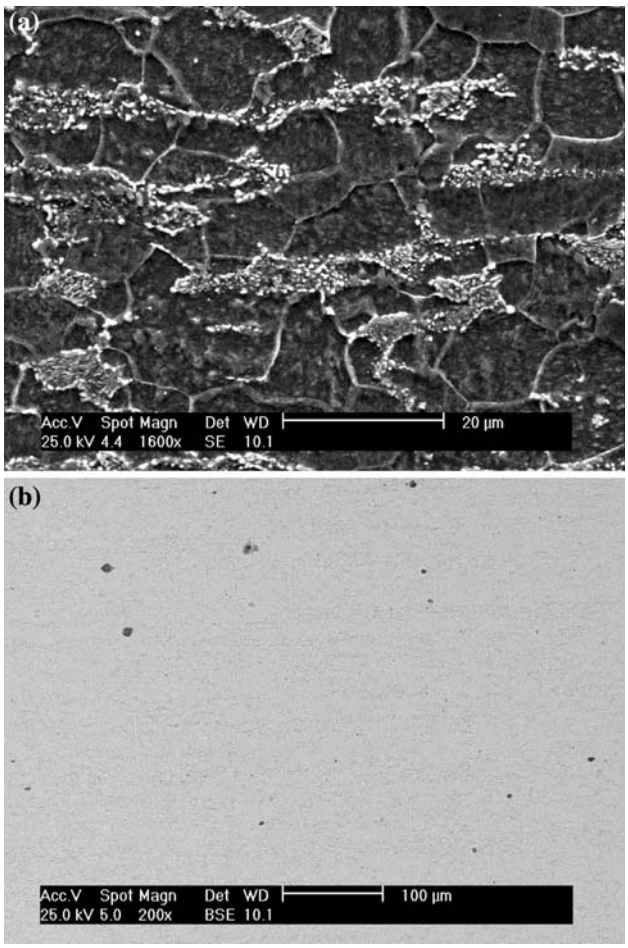

Fig. 2 SEM of the tubes in as received condition (before the bonding process): (**a**) Secondary electron (SE) image at the through-wall depths of the tube, (**b**) Backscattered electron (BSE) image at the through-wall depths of the tube

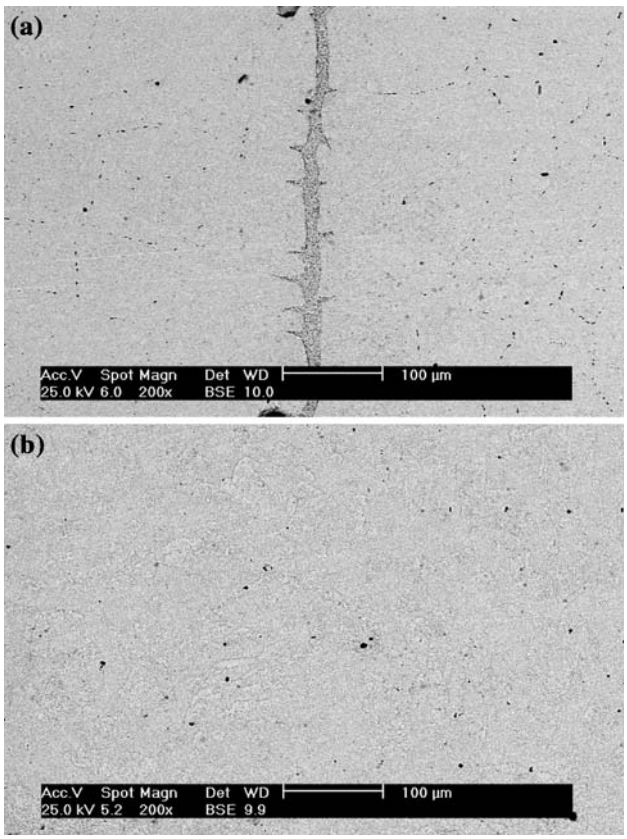

Fig. 3 SEM of the union zone for steel/iron–boron/steel bonding at 1,250 °C. The joints were performed under applied pressure of 0.8 MPa and a holding time of 3 min: (**a**) BSE image at the through-wall depths of the tube, (**b**) BSE image at 10 mm of the joint at the through-wall depths of the tube

The SEM micrographs of the tubes after the bonding process performed with $P = 0.8$ MPa and a holding time of 17 min at T_P are shown in Fig. 4. NSL is not observed at the through-wall depths of the tube. On the other hand, near the external surface of the tube, NSL is observed at the joint. The composition analyses of NSL using EDX show Fe, Al, O, Si, Ca, Mn, and Ti. A distribution of particles, with a particle size about 2–4 µm, is observed at the through-wall depths of the tube, laying primarily at prior austenite grain boundaries (Fe, Al, O, S, Ca, Mn, and Mg were detected using EDX). A random distribution of spheroidal particles, each about 4 µm or less (the presence of Fe, O, S, Ca, and Mn is detected using EDX), is found at 10 mm from the joint, at the through-wall depths of the tube.

Micrographs of the tubes after the bonding process performed with $P = 2$, 3, and 4 MPa and a holding time of 7 min at T_P, obtained using OM and SEM, are shown in Figs. 5–7, respectively.

In the case $P = 2$ MPa, traces of NSL are observed at the through-wall depths of the tube. On the other hand, near the external surface of the tube, NSL is observed at the joint. The composition analyses of NSL using EDX show Fe, Al, O, Si, and Mn. At the through-wall depths of the tube, the structure consists of ferrite (dark) and pearlite (light). A distribution of particles, each about 1 µm, is found to lie mainly at prior austenite grain boundaries (Fe, Al, O, Si, and Mn are detected using EDX). At 10 mm from the joint, at the through-wall depths of the tube, the structure consists of ferrite (dark) and pearlite (light), but the amount of pro-eutectoid ferrite is clearly lower. A random distribution of spheroidal particles, each about 5 µm or less, is observed (the presence of Fe, Al, O, Si, S, Ca, and Mg is confirmed using EDX).

In the case $P = 3$ MPa, NSL is not observed at the through-wall depths of the tube. On the other hand, near the external surface of the tube, traces of NSL are detected. The composition analyses of NSL using EDX show Fe, Al, O, Si, S, Ca, and Mn. At the through-wall depths of the tube, the structure consists of ferrite (dark), martensite-austenite

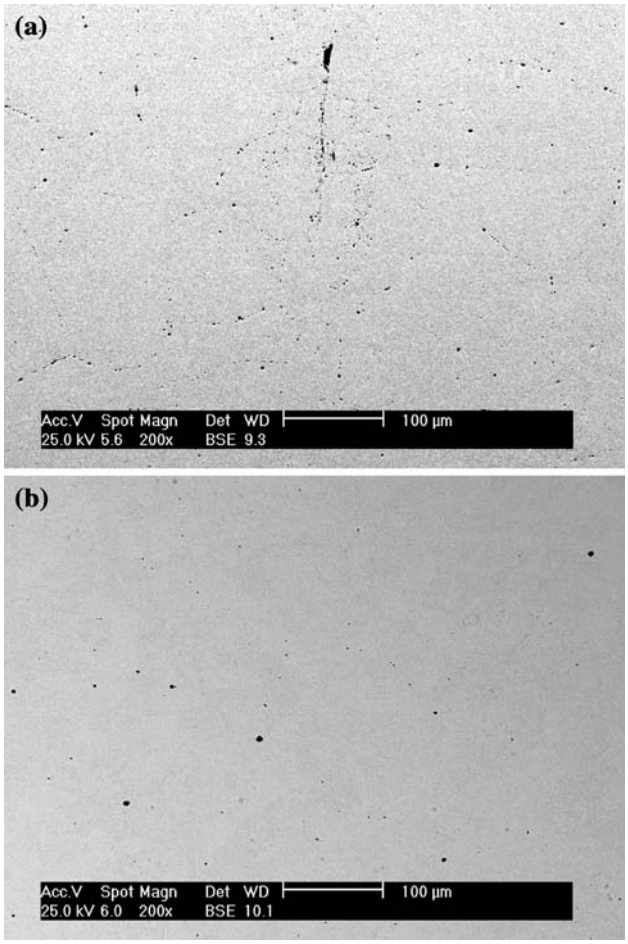

Fig. 4 SEM of the union zone for steel/iron–boron/steel bonding at 1,250 °C. The joints were performed under an applied pressure of 0.8 MPa and a holding time of 17 min: (**a**) BSE image at the through-wall depths of the tube, (**b**) BSE image at 10 mm of the joint at the through-wall depths of the tube

(MA) (gray), and pearlite (light). The presence of bainite cannot be discounted. A distribution of particles, each about 1 μm, is found to lie mainly at prior austenite grain boundaries (the presence of Fe, Al, O, and Mn is checked using EDX). At 10 mm from the joint, at the through-wall depths of the tube, the structure consists of ferrite (dark), MA (gray), and pearlite (light), but the amount of pro-eutectoid ferrite is clearly lower. The presence of bainite cannot be discounted. A random distribution of spheroidal particles, each about 4 μm or less, is observed (the presence of Fe, Al, O, S, Ca, Mn, and Mg is detected using EDX).

In the case $P = 4$ MPa, NSL is not observed at the through-wall depths of the tube. On the other hand, near the external surface of the tube, traces of NSL are detected. The composition analysis of NSL using EDX shows Fe, Al, O, and S. At the through-wall depths of the tube, the structure consists of ferrite (dark), MA (gray), and pearlite

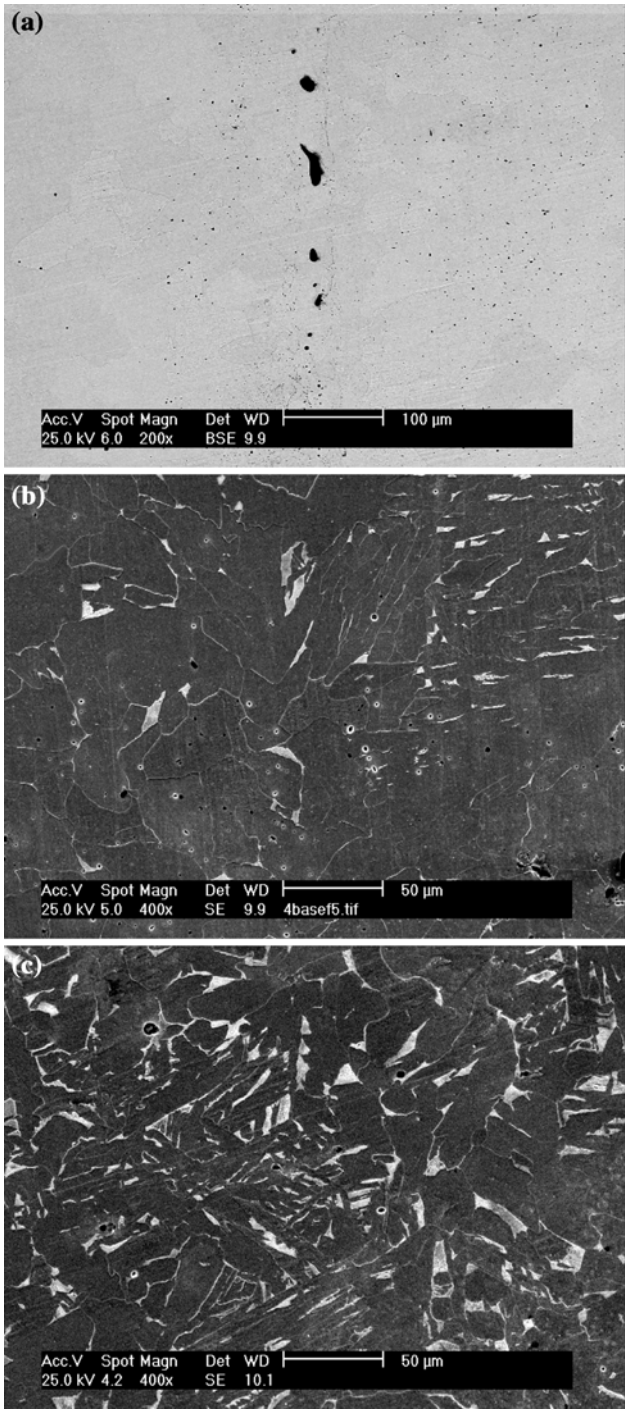

Fig. 5 SEM of the union zone for steel/iron–boron/steel bonding at 1,250 °C. The joints were performed under an applied pressure of 2 MPa and a holding time of 7 min: (**a**) BSE image at the through-wall depths of the tube, (**b**) SE image at the through-wall depths of the tube, (**c**) SE image at 10 mm of the joint at the through-wall depths of the tube

(light). The presence of bainite cannot be discounted. A distribution of particles, each about 2–3 μm in diameter, is found to lie primarily at prior austenite grain boundaries

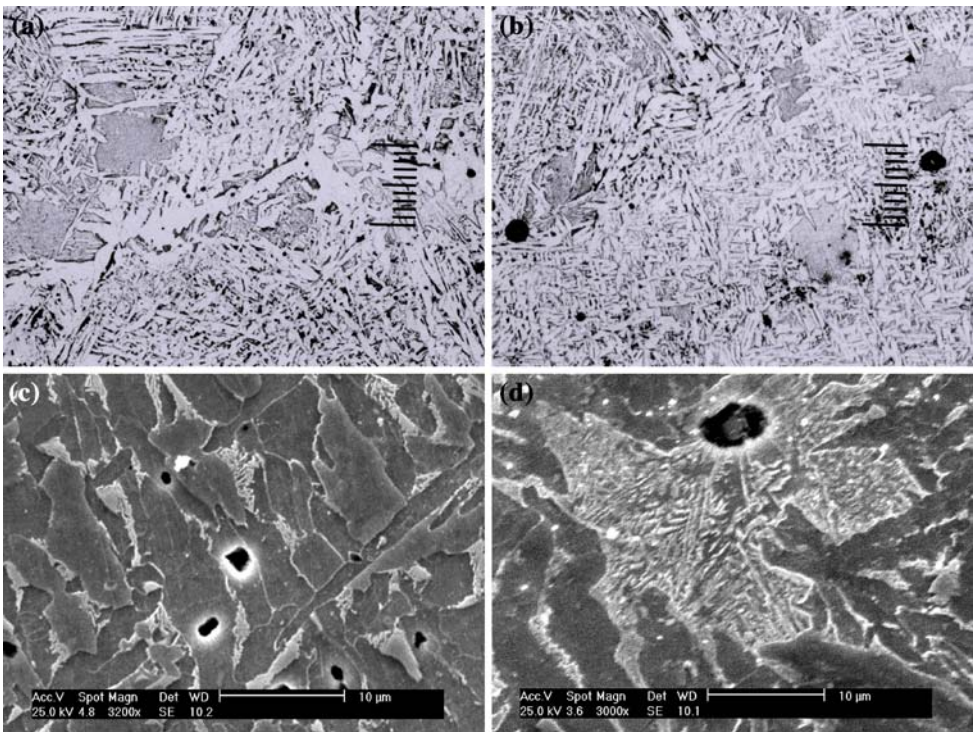

Fig. 6 Optical micrograph and SEM of the union zone for steel/iron–boron/steel bonding at 1,250 °C. The joints were performed under an applied pressure of 3 MPa and a holding time of 7 min: (**a**) Optical micrograph at the through-wall depths of the tube (full-scale: 50 µm), (**b**) Optical micrograph near the external surface of the tube (full-scale: 50 µm), (**c**) SE image at the through-wall depths of the tube, (**d**) SE image at 10 mm of the joint at the through-wall depths of the tube

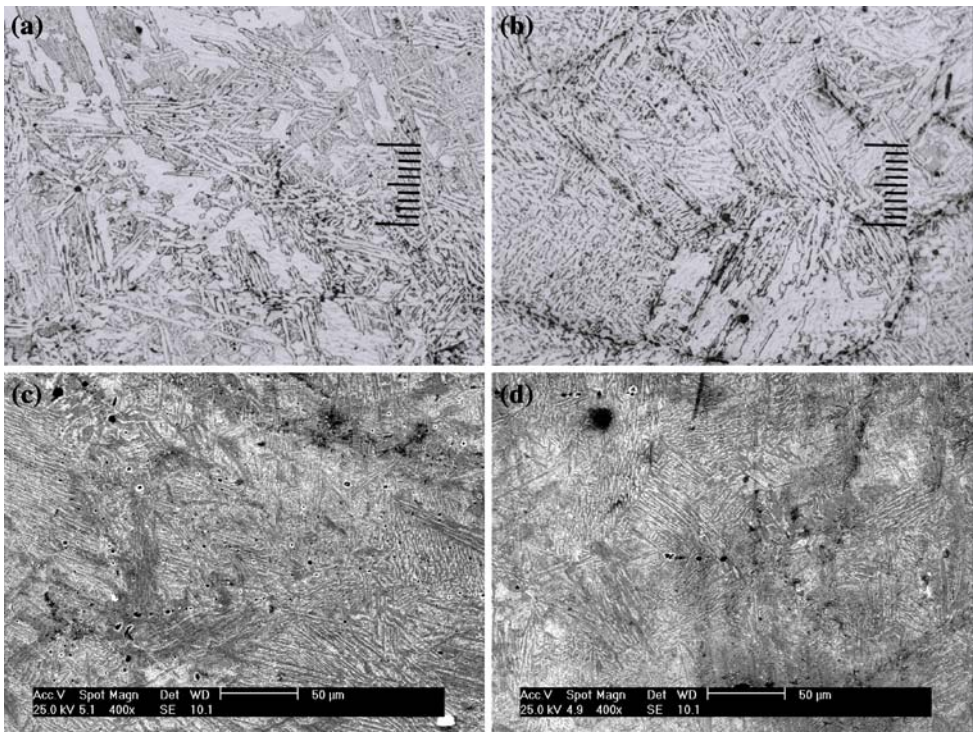

Fig. 7 Optical micrograph and SEM of the union zone for steel/iron–boron/steel bonding at 1,250 °C. The joints were performed under an applied pressure of 4 MPa and a holding time of 7 min: (**a**) Optical micrograph at the through-wall depths of the tube (full-scale: 50 µm), (**b**) Optical micrograph near the external surface of the tube (full-scale: 50 µm), (**c**) SE image at the through-wall depths of the tube, (**d**) SE image at 10 mm of the joint at the through-wall depths of the tube

(the presence of Fe, Al, O, Si, S, Ca, Mn, and Mg is detected using EDX). At 10 mm from the joint, at the through-wall depths of the tube, the structure consists of ferrite (dark), MA (gray), and pearlite (light), but the amount of pro-eutectoid ferrite is clearly lower. The presence of bainite cannot be discounted. A random distribution of spheroidal particles, each about 4 µm, is observed (the presence of Fe, Al, O, Si, S, Ca, Mn, and Mg is confirmed using EDX).

From metallographic inspection it is concluded that the bonding process ends in 7.0 min when a pressure of 4 MPa is applied, whereas the process results incomplete for the

utilized time if the applied pressure is less. For shorter time a structural separation between the joined pieces due to the presence of NSL is observed.

Discussion

Temperature holding time and profile of the joint

In the case of the bonding performed with $P = 0.8$ MPa and a holding time of 17 min at T_P, the isothermal solidification was completed at the through-wall depths of the tube. Near the external surface of the tube, we found NSL along the joint (see Fig. 4).

On the bonding performed with a pressure of 0.8 MPa and a holding time of 3 min at T_P, we found NSL along the whole joint, completely separating both base metals (see Fig. 3). Paulonis and colleagues [6] using Inconel 713c as base metal, pressures less than 0.1 MPa and bonding temperatures T_P between 1,100 and 1,200 °C, obtained NSL along the whole joint for insufficient holding times at T_P. As a result, for an insufficient holding time at T_P, NSL forms a continuous phase that avoids the contact between both base metals.

In the cases of bonds performed with a holding time of 7 min at T_P, and pressures of 2 and 3 MPa (see Figs. 5 and 6), we found that as pressure was increased, the amount of NSL decreased along the joint. The comparison of bonds performed with pressures of 3 and 4 MPa (see Figs. 6 and 7) shows the amount of NSL that remained along the joint was almost the same.

On other hand, we found plastic deformation at the joint in all the bonds. This is similar to the findings of Hamada et al. [9] who performed bonds with low alloy steel tubes as base metal, a pressure of 10 MPa and a holding time of 5 min at $T_P = 1{,}250$ °C. If we suppose a uniform plastic deformation at the joint, taking into account that plastic flow occurs at constant volume, we can estimate the true strain ε using the following expression:

$$\varepsilon = \mathrm{In}(A_\mathrm{f}/A_\mathrm{o}),$$

where A_f and A_o are the final and initial cross-sectional area, respectively.

Finally, we obtain a strain ε of 0.05, 0.07, and 0.19 for the bonds with a pressure of 2, 3, and 4 Mpa, respectively.

Chemical composition and distribution of particles

The composition of the particles was examined by EDX, obtaining similar compositions in all the specimens, generally formed of Al_2O_3, CaS, $MgAl_2O_4$, MnS, MnO, and SiO_2. The high concentration of Fe measured on some particles comes from the Fe matrix of the steel.

The particle distribution at 10 mm from the joint is random. The same distribution is also observed on the tube in the as received condition. The size of the particles is 6 μm or less.

The amount of particles is greater at the joint in all the bonds. The particles, with a size between 1 and 5 μm, are located preferentially at prior austenite grain boundaries.

Composition of the NSL

The chemical composition of the NSL at the joint was analyzed by EDX. At the through-wall depths position, we can observe two cases:

1 When there is residual NSL.
2 When there is a continuous phase of NSL at the joint.

The first case is observed in the bonds at the following conditions:

- Pressure of 0.8 MPa and a holding time of 17 min at T_P.
- Pressure of 2 MPa and a holding time of 7 min at T_P.
- Pressure of 3 MPa and a holding time of 7 min at T_P.
- Pressure of 4 MPa and a holding time of 7 min at T_P.

For these bonding, EDX shows the presence of O, Al, Mn, Si, S, Ca, and Ti, in addition to Fe and B (B cannot be discounted), probably forming:

- SiO_2, MnO, and Al_2O_3 on the bonding performed with a pressure of 0.8 MPa and a holding time of 17 min at T_P.
- Al_2O_3, SiO_2, and MnO on the bonding performed with a pressure of 2 MPa and a holding time of 7 min at T_P.
- Al_2O_3, SiO_2, CaS, and MnO on the bonding performed with a pressure of 3 MPa and a holding time of 7 min at T_P.
- Al_2O_3 on the bonding performed with a pressure of 4 MPa and a holding time of 7 min at T_P.

The NSL has a chemical composition similar to the particles along the tube (in the as received condition).

The second case is observed in the bonds performed with a pressure of 0.8 MPa and a holding time of 3 min at T_P. Although EDX analysis only detected Fe, the presence of B cannot be discounted.

This behavior can be explained as follows. During the isothermal solidification, any insoluble particles trapped within the liquid phase are dragged by the interfaces and, despite the fact that the liquid gap is shrinking, remain within the liquid phase [13]. Now we consider the first case. The isothermal solidification has almost finished, and just remains of liquid are observed along the joint with all the particles that were dragged by the interfaces. The solidification ends upon cooling, that is, the remaining

liquid solidifies with all the particles to form a new phase with a chemical composition similar to that of the particles along the tubes. Considering the second case, the isothermal solidification is incomplete because of the short holding time at T_P. Therefore, the chemical composition of the solidified liquid upon cooling should be similar to the composition filler metal. This is in correspondence with the EDX analysis of the NSL, which has detected Fe.

Microstructure

The effect of the pressure on the microstructure can be studied in the bonds performed with pressure of 2, 3, 4 MPa (with a holding time of 7 min). Micrographs show that if pressure increases, the amount of pro-eutectoid ferrite decreases in both: at the joint and at 10 mm from the joint. In other words, the amount of other constituents (martensite-austenite) of the steel increases with pressure. We found, mainly:

- Pearlite with a pressure of 2 MPa.
- Pearlite and MA with a pressure of 3 MPa.
- MA with a pressure of 4 MPa.

Therefore, as the cooling rate is the same in all the bonds, the austenite transformation is delayed by pressure increasing, that is, pressure increases the hardenability of the steel. This fact was observed by Nilan [14] in Cr–Ni steels with pressure from 1 bar to 24 kbar. He reported a shift to longer times of the isothermal transformations curves.

Micrographs also show the hardenability at the joint is lesser than the hardenability at 10 mm from the joint. This fact can be explained according to the joint exhibits:

- A higher amount of B from the filler metal.
- The presence of compression plastic deformation.

Firstly, it is well known that the presence of soluble B in steels (at least 0.0005 wt.%), produces an increase in the hardenability [15]. On the other hand, Smith and Siebert [16] reported that the compression plastic deformation produces a decrease in the hardenability. Therefore, the hardenability decrease of the joint (compared with the hardenability at 10 mm from the joint) could be explained considering the amount of soluble B could be negligible (most of B is forming particles), or that the effect of the compression plastic deformation could be higher than the effect of the presence of soluble B. To sum up, the effect of the compression plastic deformation could prevail at the joint zone.

Conclusions

TLPB processes have been performed under pressure in steel using an Fe–B interlayer. We can conclude the bonding process ends in 7.0 min if a pressure of 4 MPa is applied, whereas the process results incomplete if less pressure is applied.

Plastic deformation at the joint is observed. Micrographs show that if pressure increases, the amount of pro-eutectoid ferrite decreases. Therefore, an increase in the hardenability of the steel is observed with pressure. This fact could be due to the effect of compression plastic deformation that prevails at the joint zone over the effect of the presence of B. In the case that the NSL is residual, NSL has a chemical composition similar to that of the particles of the tube in received condition.

References

1. Sinclair CW, Purdy GR, Morral JE (2000) Metall Mater Trans A 31A:1187. doi:10.1007/s11661-000-0114-2
2. Ohsasa K, Shinmura T, Narita T (1999) J Phase Equilib 20(3): 199. doi:10.1361/105497199770335721
3. Sinclair CW (1999) J Phase Equilib 20(4):361. doi:10.1361/105497199770340888
4. MacDonald WD, Eagar TW (1992) Annu Rev Mater Sci 22:23
5. Ikawa H, Nakao Y, Isai T (1979) Trans Jpn Weld Soc 10(1):25
6. Duvall DS, Owczarski WA, Paulonis DF (1974) Weld J 53:203
7. Tuah-Poku I, Dollar M, Massalski TB (1988) Metall Trans A 19A:675
8. Kishi S, Maenosono T, Sato M (1999) US Patent number 5875954
9. Hamada M, Fukadal Y, Hueda M, Komizo Y (2000) US Patent number 6059175
10. Shimizu T, Horio H, Kito K, Inagaki S, Yamada R (2003) US Patent number 6592154 B2
11. Di Luozzo N, Fontana M, Arcondo B (2007) J Mater Sci 42(11):4044. doi:10.1007/s10853-006-0190-9
12. Cain SR, Wilcox JR, Venkatraman R (1997) Acta Mater 45(2):701. doi:10.1016/S1359-6454(96)00188-7
13. Shirzadi AA, Wallach ER (1999) Acta Mater 47:3551. doi:10.1016/S1359-6454(99)00234-7
14. Nilan TG (1967) AIME Met Soc Trans 239(6):898
15. Thelning KE (1979) Boron in steel, Milwaukee, WI, p 127
16. Smith YE, Siebert CA (1971) Metall Trans 2:1711. doi:10.1007/BF02663352